Journal of Materials Science and Engineering 5 (2011) 212-219

Nonlinear Flexural Behavior and Moment Curvature Response of Epoxy Resin Using Digital Image Correlation Technique

Masoud Yekani Fard, Yingtao Liu and Aditi Chattopadhyay

Department of Mechanical Engineering, School of Engineering of Matter, Transport and Energy, Arizona State University, Tempe, AZ 85287-6106, USA

Received: August 31, 2010 / Accepted: October 07, 2010 / Published: February 10, 2011.

Abstract: The effect of local strain and stress distribution in the polymeric material under out of plane loading is of interest in many applications. Flexural testing of the epoxy resins is necessary to evaluate their mechanical behavior. In this paper, the flexural response of epoxy resin Epon E 863 and hardener EPI-CURE 3290 has been investigated in three point bending (3PB) at different strain rates. Beam specimens with rectangular cross sections, different lengths and span to depth ratios were tested at their mid point. Samples had either a quarter deep notch or a groove at their mid points. Strain fields within the beam structure were determined using digital image correlation technique. Load deflection curves at different load speeds were obtained. Limit of proportionality (LOP), modulus of rupture (MOR), initial slope of the load-deflection curve, and slope of load deflection curve after the LOP point were extracted. The nonlinear moment curvature behavior has been obtained. The results show that a digital image correlation can accurately categorize the material response of an epoxy resin for flexural loading. Results clearly display the strain rate effects on the material response.

Key words: Flexure, epoxy resin, load deflection, digital image correlation technique.

1. Introduction

Mechanical properties of fiber reinforced polymeric composites are of increasing interest as their applications in mechanical and civil industries become widespread. These properties are dominated by those of the matrix, so the role of epoxy resin in polymeric matrix composites is extremely important due to the nonlinear nature of polymer behavior. Chou et al. [1] studied the stress strain compression behavior of polymethyl methacrylate (PMMA), cellulose acetate butyrate, polypropylene and nylon 66 over a wide range of strain rates using a medium strain-rate machine and a split Hopkinson pressure bar. The compressive yield behavior of two major monomers, Araldite MY721 and Araldite MY0510 were investigated as a function of temperature and strain rate [2]. Three point bending (3PB) tests were used to study the different environmental and aging effects on mechanical properties of five different types of fiber posts by Mannocci et al. [3]. Fiber posts consist of fibers such as carbon, quartz, silica or glass in a matrix based resin. Fergusson et al. [4] used digital speckle photogrammetry technique to study the effect of defects on flexural behavior of sandwich composite structures. Composite structures are usually subjected to large flexural loadings, so the flexural behavior of these structures and their constituents are critical to their use. Although there is a large body of literature on the mechanical and thermal properties of epoxy [5-12], the effect of stress gradient in tensile and compressive peak stress and the entire stress strain regime has not been paid enough attention. In this study, 3PB was

Corresponding author: Masoud Yekani Fard (1971-), male, research associate, research fields: solid mechanics, mechanic of material, fracture mechanics and numerical simulation. E-mail: masoud.yekanifard@asu.edu.

selected as the loading technique and the strength and ductility of the un-reinforced epoxy resin under flexure have been investigated. Notch or groove at the middle of the beam makes failure to happen at the location of initial notch or groove as the region at the location of notch or groove would be subjected to high stress values. This makes strain determination of the central region by non-contact digital image correlation technique possible. Conventional methods such as strain gauges for determining strain are not sufficient for evaluation of the strain field in bending samples as they provide information only at the location of strain gage. In addition, strain gages attached to specimen might result in stress concentration and premature failure. Digital image correlation technique was used in this investigation as it is a reliable technique to determine the strain field across and along the sample as opposed to strain gauge. The results will be used to study stress strain model of polymeric materials.

2. Experiment

The materials used in this study was resin Epon 863 with a hardener EPI-CURE 3290 using a 100/27 weight ratio. ASTM standard D790 [13] section 7 was consulted for bending samples. Beams with length 60 mm and 90 mm were tested over a simply supported span of 50 mm and 78 mm, respectively and were loaded at the midpoint. All the samples initially had quarter deep notches at the middle of the beam, but half of the samples were modified by cutting out the material around the notch and making a groove. The geometry and dimensions of the samples and the modified samples are shown in Fig. 1 and Table 1. Bending tests were performed using a 3PB fixture, an electrical desktop testing machine, and a digital image correlation technique (ARAMIS 4M) as shown in Fig. 2. An interface load cell (interface model SM-1000) was used to measure the axial load.

All tests were conducted in displacement control and ambient environmental conditions. Axial strain rates achieved ranged from 26 μstr/sec to 550 μstr/sec. The loading rates corresponding to desired strain rates were calculated approximately based on the elastic linear assumption and geometry of samples as shown in Eq. (1).

$$\frac{d\delta}{dt} = \frac{S^2}{6h}\frac{d\varepsilon}{dt} \tag{1}$$

where δ is deflection at the mid-span, ε is the axial strain, S is span and h is the thickness of the beam. The supporting and loading steel rods have a radius of 6.5 mm. A stochastic spray pattern was applied to the surface of the beam between two supports. This was done by first applying a white base coat with spray paint followed by a dispersion of fine black dots. The ARAMIS system which uses digital image correlation enables non contact measurement of displacement and strain fields. The technique uses one or two digital cameras depending on whether two dimensional or three dimensional strain fields are to be observed. A reference image has to be taken while the sample is unloaded, and all the images taken during the test would be referenced against the first image. There are post processing features available within the system for determination of axial and shear strains in any given direction. The load-deformation relationship was found using the optical system through triggering option between the load cell and optical system.

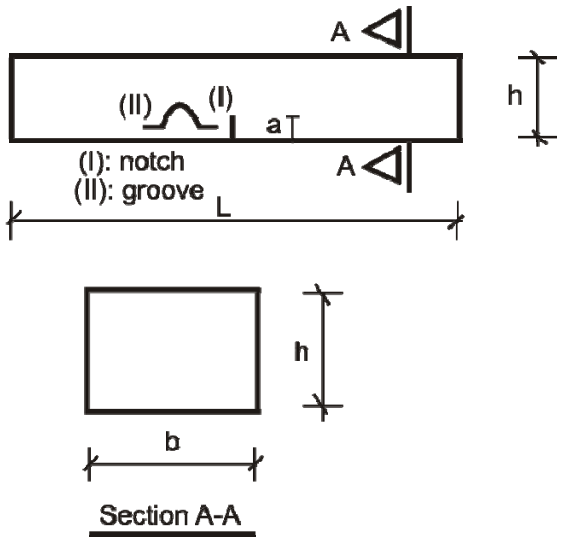

Fig. 1 Bending samples with rectangular cross sections.

Table 1 Average dimensions of bending samples.

Type	Initial imperfection	b (mm)	h (mm)	a (mm)	L (mm)	S (mm)	S/h
B1, B1m	B1m: groove	10	4	1.1	60	50	12.5
B2, B2m	B2m: groove	4	10	3.2	60	50	5
B3, B3m	B3m: groove	12	4	1.1	90	78*	19.5
B4, B4m	B4m: groove	4	12	3.2	90	78*	6.5

* Span is 68mm in samples B_3_1 and B_4_1.

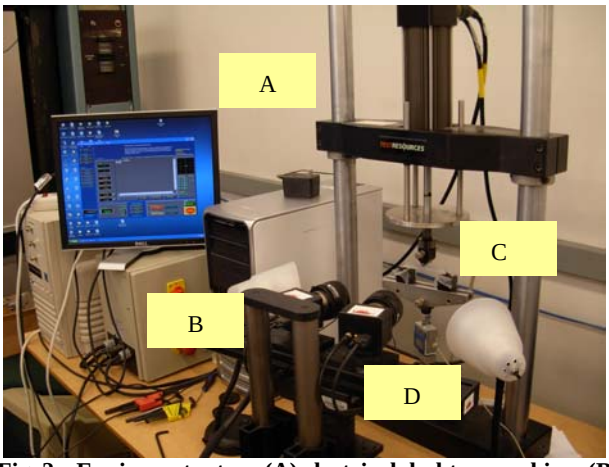

Fig. 2 Equipment setup: (A) electrical desktop machine; (B) ARAMIS; (C) 3PB fixture; and (D) interface load cell.

3. Results and Discussion

3.1 Load Deflection

The relationship between shear force and the differential of the bending moment within the beam, and the relationship between axial stress and applied load are shown in Eqs. (2) and (3) [14]. *V* and *M* are shear force and bending moment respectively. *P* is the applied load in 3PB, *S* is the span of the beam, and *b*, *h* are cross section dimensions.

$$V = \frac{dM}{dx} \tag{2}$$

$$\sigma = \frac{3PS}{2bh^2} \tag{3}$$

Changing the sign of shear stress at the mid span could be confirmed by results from digital image correlation technique. The region with stress concentration lies directly below the loading nose as a result of the compression of surface of the specimen by the loading nose. The bending moment would rise linearly from zero at the supports to the maximum value at location of the loading nose. Fig. 3 shows the load deflection curves of sample types B_1 and B_1m under monotonic 3PB test at different speeds from 0.49 mm/min to 4.74 mm/min at room temperature. While sample B_1-1 with notch failed in the ascending part of the load deflection curve, modified samples B_1m-3, B_1m-5, and B_1m-6 with groove failed after the modulus of rupture (MOR) point and at the start of deflection softening regime. Samples B_1-2 and B_1m-4 failed prematurely. The same trend has been observed for bending sample types B_3 and B_3m as shown in Fig. 4. A possible cause for the premature failure in samples B_1 and B_3 is the stress concentration at the location of notch as fracture occurred along a straight line as shown in Fig. 5. Data of samples type 1 and 3 shows that deflection at failure in notched samples is around 60% of the one in grooved samples. The load deflection behavior for sample types B_2, B_2m, and B_4, B_4m are shown in

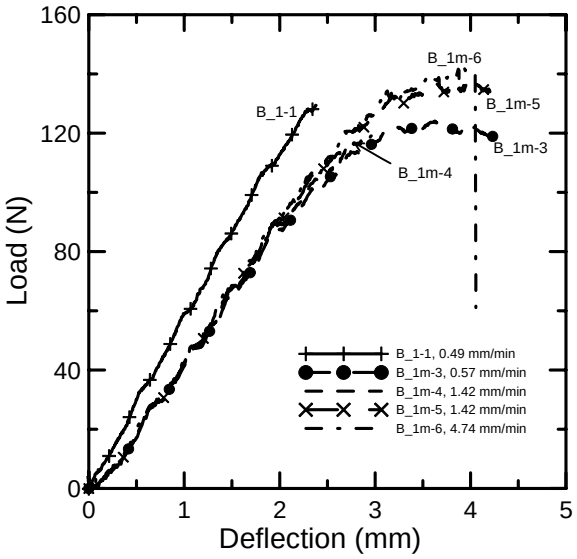

Fig. 3 Load deflection for sample types B_1 and B_1m.

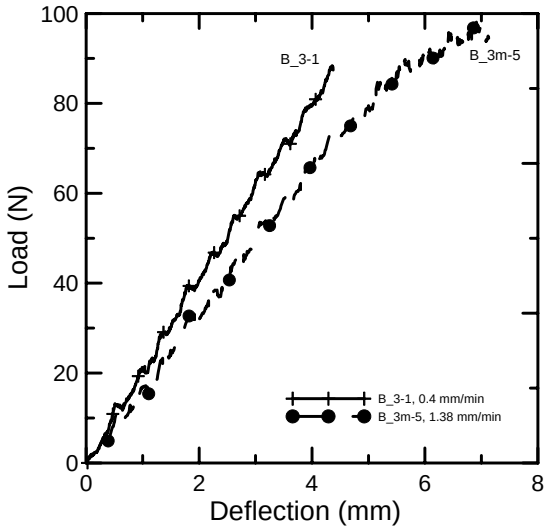

Fig. 4 Load deflection curves of sample types B_3 and B_3m.

Fig. 5 Fracture surface of the broken samples B_1-2 and B_2-2.

Figs. 6 and 7, respectively. The load initially increases proportionally to deflection before passing through a knee point called limit of proportionality (LOP). The load keeps increasing with a reduced slope up to the maximum point known as MOR followed by a deflection softening and final failure. Brittle failure occurred after a considerable amount of plastic deformation in most of the samples. Mechanical characteristics of bending samples are shown in Table 2.

The initial stiffness was measured as the slope of the load deflection curve in the linear region between 0.3 mm and 1.00 mm. Samples with groove show a less initial stiffness than samples with notch even for the same speed. Beam types B_2, B_2m, B_4, and B_4m show more plastic deformation and less premature failure than the other types of samples. This is mainly due to the higher thickness of these samples and consequently, lower effect of stress concentration around the sharp notch at failure. This fact indicates that stress concentration plays a major role in the type

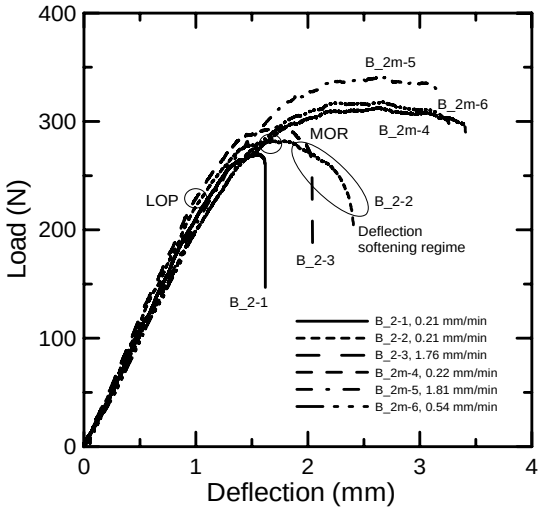

Fig. 6 Load deflection curves of sample types B_2 and B_2m.

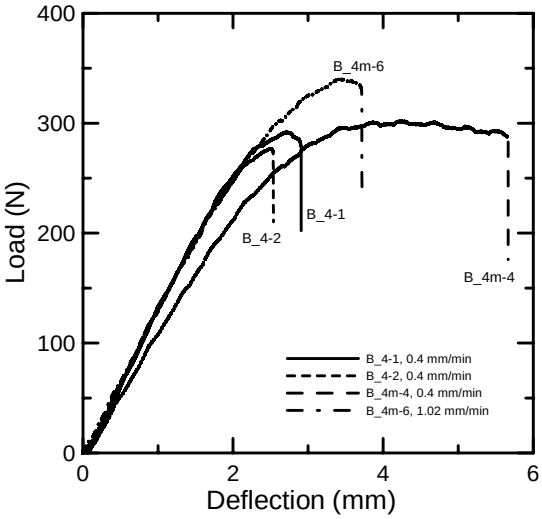

Fig. 7 Load deflection curves for sample types B_4 and B_4m.

of fracture and may overshadow the strain rate effect on MOR, degree of nonlinearity and the entire response of the material. Fig. 6 shows that samples B_2m-4 to B_2m-6 illustrate more ductile behavior than samples B_2-1 to B_2-3. Results indicate that MOR of the material under higher loading rates is higher than its lower rate counterpart (111.9 MPa in sample B_2-3 compared with 106.08 MPa for sample B_2-2). It was observed that increasing the rate of loading increases slightly the initial stiffness of the sample. Samples B_2 and B_2m were fractured after the peak load and after showing a considerable amount of softening. Beam type 4 with notch and groove (B_4, and B_4m) were

Table 2 Mechanical characteristics for load deflection response.

Sample	Initial slope (N/mm)	Slope of post LOP (N/mm)	MOR (MPa)	Δ_{MOR} (mm)	LOP (MPa)	Δ_{LOP} (mm)	Def. at Failure (mm)
B_1-1	57.49	n.a	n.a	n.a	87.2	1.90	2.45
B_1-2	60.0	n.a	n.a	n.a	n.a	n.a	1.77
B_1m-3	45.22	18.31	117.7	3.6	96.5	2.38	4.26
B_1m-4	45.62	n.a	n.a	n.a	97.8	2.39	3.01
B_1m-5	47.56	18.90	118.5	3.99	92.7	2.4	4.24
B_1m-6	48.11	21.99	120.1	3.94	90.3	2.34	4.12
B_2-1	219.93	115.04	100.3	1.54	73.9	0.92	1.67
B_2-2	224.09	90.7	106.1	1.69	81.4	0.96	2.44
B_2-3	230.8	96.6	111.9	1.72	83.3	0.94	2.16
B_2m-4	199.4	70.3	121.2	2.63	76.0	0.97	3.46
B_2m-5	202.05	76.9	132.2	2.7	83.3	1.05	3.14
B_2m-6	201.6	68.8	124.7	2.67	80.8	1.03	3.27
B_3-1	20.3	n.a	n.a	n.a	n.a	n.a	4.4
B_3-2	18.83	n.a	n.a	n.a	n.a	n.a	4.89
B_3-3	19.46	n.a	n.a	n.a	n.a	n.a	3.86
B_3m-4	17.2	12.07	115.4	6.41	93.4	4.83	6.41
B_3m-5	17.44	12.42	116.6	6.88	90.0	4.84	7.17
B_3m-6	18.27	13.2	110.5	6.6	88.9	4.67	6.6
B_4-1	141.2	79.7	92.0	2.7	61.0	1.47	3.01
B_4-2	135.7	n.a	n.a	n.a	63.7	1.34	2.61
B_4-3	141.19	n.a	n.a	n.a	65.3	1.29	2.29
B_4m-4	112.5	44.8	111.6	4.24	70.4	1.75	5.72
B_4m-5	120.0	n.a	n.a	n.a	n.a	n.a	2.07
B_4m-6	127.2	79.4	125.7	3.39	81.4	1.73	3.78

tested at two speeds of 0.4 mm/min and 1.02 mm/min. Samples B_4-2, B_4-3, and B_4m-5 failed prematurely before reaching their load capacity. Results of B_4m-4 and B_4m-6 show that increasing the speed of loading by three times increases the initial stiffness and MOR by around 13%. Fig. 8 shows the strain at the top and bottom layer at the middle of the beam vs. displacement at the mid span. As the ARAMIS system was not able to resolve the very top and bottom surfaces during deformation, strain readings provided by the digital image correlation system were taken as close to the surfaces as possible. As the axial strains in the layers decreases with distance from the surface, the strain observed by non-contact digital image system were slightly less than the precise strains. Results show that increasing the displacement increases the axial strains at top and bottom layers of the beam. Increasing the strain in top and bottom layers is more symmetric in

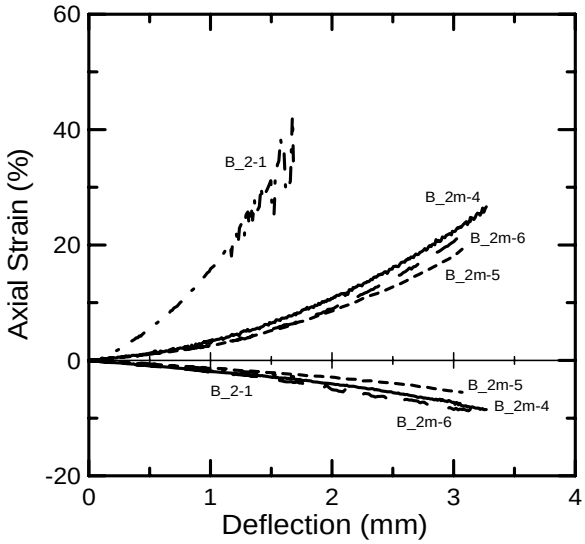

Fig. 8 Axial strain at top and bottom layers vs. deflection at the center.

beams with groove than in beams with notch. Fig. 9 shows the effect of stress concentration on the axial strain field at the middle of the beam for B_2m-5 with

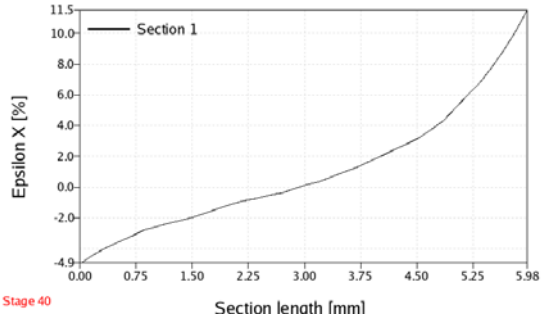

Fig. 9 Effect of stress concentration on distribution of ε_x in beam 2m-5.

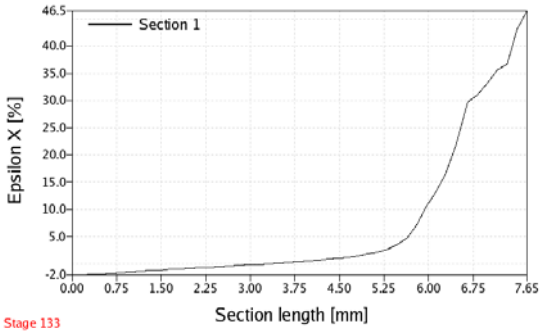

Fig. 10 Distribution of ε_x in beam 2-2.

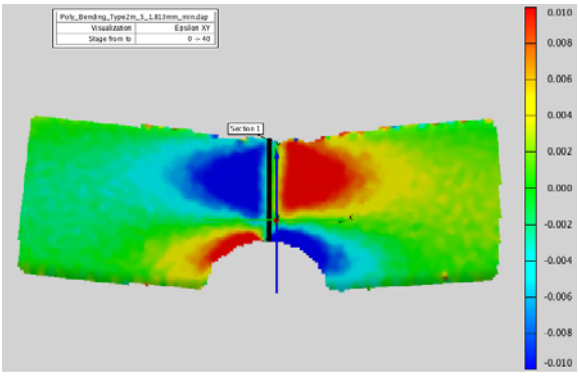

Fig. 11 Shear strain distribution at the maximum load capacity for B_2m-5.

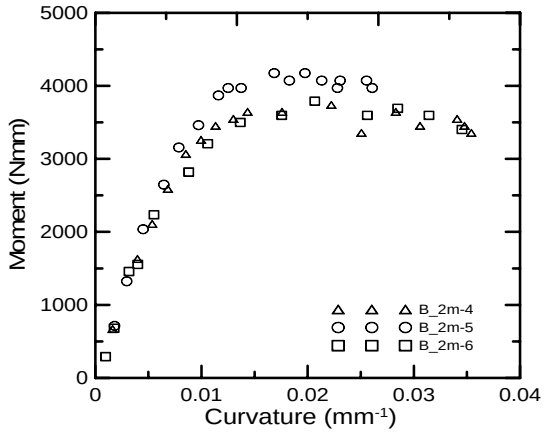

Fig. 12 Moment curvature diagram in beams B_2m-4, B_2m-5, and B_2m-6.

groove, while Fig. 10 illustrates the extreme effect of stress concentration due to notch on axial strain distributions at the middle of beam B_2-2. Results show that axial strain distribution in notched samples extremely violates the linear assumption due to stress concentration. It is clear that higher thickness with groove at the middle will increase the degree of nonlinearity and softening in the material behavior. Fig. 11 illustrates the shear strain distribution under the loading nose at the load capacity stage for beam B_2m-5. Results show that maximum shear strain is less than 1% in the beams. Fig. 12 presents clearly the nonlinearity in the moment curvature diagram and the effect of softening in moment curvature response.

3.2 Mechanical Properties

Flexural specimens show a nonlinear material behavior and plastic deformation before failure. Fig. 13 illustrates the relation between initial slope of load deflection curve at room temperature and rate of loading. There is a slight increment in the initial slopes as speed of loading increases in most of the samples except B_3.

It is to be noted that the span in B_3-1 and B_4-1 was 68 mm (10mm less than the other beams). Results illustrate that MOR increases approximately linearly with increasing speed of loading except in B_3m where the increase in MOR followed by a decrease at 3.45 mm/min as shown in Fig. 14. This decrease might be due to the premature failure of sample B_3m-6. Results show no specific trend in variation of LOP vs. load speed. Quantitative estimate of stress at the LOP point based on stress at the MOR point for all load speeds is made in Fig. 15. Results show that LOP stress is around 72% of MOR stress. This can be compared to the limit of stress in the linear part of tension and compression stress strain curve under monotonic uniaxial loading to examine the effect of out of plane loading which is currently under investigation by the authors. The fracture of the some of the broken specimens occurred along the plane perpendicular to the direction of the

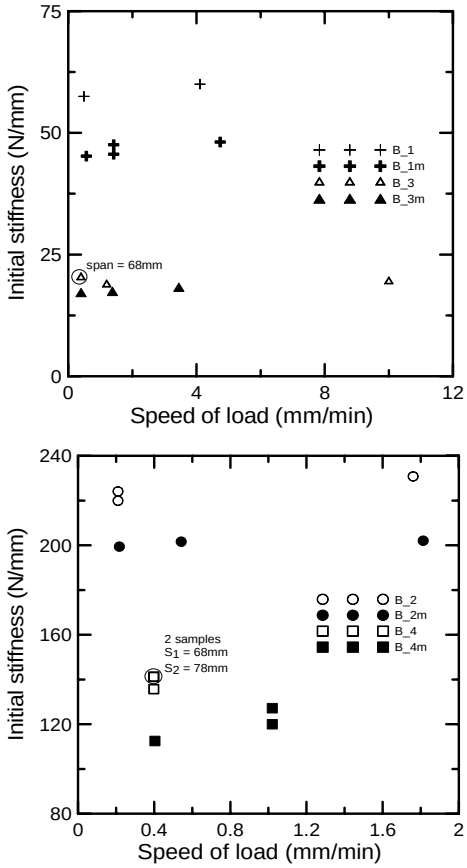

Fig. 13 Variations of initial stiffness with rate of loading (Note: symbols enclosed in circle indicate overlapping data).

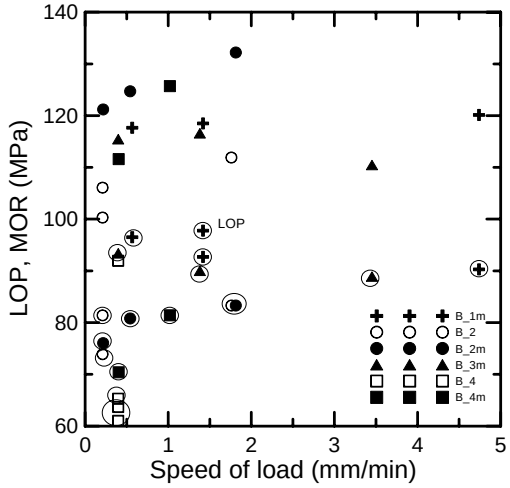

Fig. 14 Variations of LOP and MOR with rate of loading (Note: symbols enclosed in circle indicate LOPs).

maximum tensile stress on the tension side, and for the others under an angle of about 45° to the longitudinal direction and showed a bump shape as shown in Fig. 5. This type of failure was observed after a quite amount of plastic deformation. It is to be noted that fracture

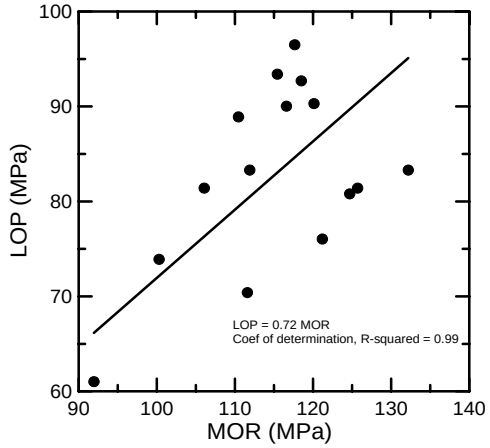

Fig. 15 Variations of LOP with MOR in flexure at different load speeds.

usually occurs at the maximum principal tensile stress. Stress concentration has been observed around the loading nose in some of the samples. The effect of the stress concentration on the stress distribution has not been studied in this paper.

4. Conclusions

In this study, the flexural response of Epon 863 and hardener EPI-CURE 3290 has been investigated in three point bending (3PB) at different strain rates using digital image correlation technique. Digital image correlation system could accurately provide strain field information in 3PB tests of polymeric materials. Stress concentration due to notch changed the strain distribution in the beams while groove improved the stress concentration problem considerably. Results do agree with the beam bending theory and the consequent lack of shear strain in the beams. Results showed that increasing the rate of loading increases the initial stiffness and modulus of rupture (MOR). Results also show the nonlinear nature of moment curvature response and the effect of softening in the post peak region. The obtained moment curvature response could be used as material data for nonlinear numerical simulations. Quantitative estimates show that the stress at limit of proportionality (LOP) is around 72% of stress at MOR. The results of this study will be used as a validation tool in constitutive model development for out of plane loading in polymeric materials.

Acknowledgments

The authors gratefully acknowledge the support of this research by the Army Research Office, AMSRD-ARL-RO-SI Proposal Number: 49008-EG, Agreement Number: W911NF-07-1-0132, Program Manager: COL. Reed F. Young. We also thank Dr. Dallas Kingsbury from ASU for assistance in conducting the tests.

References

[1] S.C. Chou, K.D. Robertson, The effect of strain rate and heat developed during deformation on the stress-strain curve of plastics, Exp. Mech. 13 (1973) 422-432.

[2] S. Behzadi, F.R. Jones, Yield behavior of model epoxy matrices for fiber reinforced composites: Effect of strain rate and temperature, J. Macromol Sci. B: Phys. 44 (2005) 993-1005.

[3] F. Mannocci, M. Sherriff, T.F. Watson, Three-point bending test of fiber posts, J. Endodont 27 (2001) 758-761.

[4] A.D. Fergusson, A. Puri, A. Morris, J.P. Dear, Flexural testing of composite sandwich structures with digital speckle photogrammetry, Appl. Mech. Mater. 5-6 (2006) 135-144.

[5] C.P. Buckley, J. Harding, Deformation of thermosetting resins at impact rates of strain, part I: Experimental study, J. Mech. Phys. Solids 49 (2001) 1517-1538.

[6] C.P. Buckley, P.J. Dooling, Deformation of thermosetting resins at impact rates of strain, part 2: constitutive model with rejuvenation, J. Mech. Phys. Solids 52 (2004) 2355-2377.

[7] M.Z.S. Khan, G. Simpson, A comparison of the mechanical properties in compression of two resin systems, Mater. Lett. 52 (2002) 173-179.

[8] A. Gilat, R.K. Goldberg, G.D. Roberts, Strain rate sensitivity of epoxy resin in tensile and shear loading, J. Aerospace Eng. ASCE (2007) 75-89.

[9] J.L. Jordan, J.R. Foley, C.R. Siviour, Mechanical properties of epon 826/DEA epoxy, Mech Time-Depend Mater 12 (2008) 249-272.

[10] J.D. Littell, C.R. Ruggeri, R.K. Goldberg, G.D. Roberts, W.A. Arnold, W.K. Binienda, Measurement of epoxy resin tension, compression, and shear stress-strain curves over a wide range of strain rates using small test specimens, J. Aerospace Eng. ASCE (2008) 162-173.

[11] V. Kozey, S. Kumar, Compressive behavior of epoxy resins, in: International SAMPE Technical Conference, 1994.

[12] M. Miwa, A. Takeno, Strain rate and temperature dependence of shear properties of epoxy resin, J. Mater. Science 30 (1995) 1760-1765.

[13] ASTM D790, Standard test method for flexural properties of unreinforced and reinforced plastics and electrical insulatins materials, 2003.

[14] S.P. Timoshenko, J.M. Gere, Mechanical of Materials (3rd ed.), PWS-KENT Publishing Company, 2004.